

Journal of Biomedical Optics

SPIEDigitalLibrary.org/jbo

Fluorescence-based surface magnifying chromoendoscopy and optical coherence tomography endoscope

R. Andrew Wall
Jennifer K. Barton



SPIE

Fluorescence-based surface magnifying chromoendoscopy and optical coherence tomography endoscope

R. Andrew Wall^a and Jennifer K. Barton^{a,b}

^aThe University of Arizona, College of Optical Sciences, 1630 E. University Boulevard, Tucson, Arizona 85721

^bThe University of Arizona, Department of Biomedical Engineering, 1127 E. James E. Rogers Way, Tucson, Arizona 85721

Abstract. A side-viewing, 2.3-mm diameter, surface magnifying chromoendoscopy-optical coherence tomography (SMC-OCT) endoscope has been designed for simultaneous, nondestructive surface fluorescence visualization and cross-sectional imaging. We apply this endoscope to *in vivo* examination of the mouse colon. A 30,000 element fiber bundle is combined with single mode fibers, for SMC and OCT imaging, respectively. The distal optics consist of a gradient-index lens and spacer to provide a 1× magnification at a working distance of 1.58 mm in air, necessary to image the sample through a 0.23-mm thick outer glass envelope, and an aluminized right-angle prism fixed to the distal end of the gradient-index lens assembly. The resulting 1:1 imaging system is capable of 3.9- μm lateral and 2.3- μm axial resolution in the OCT channel, and 125-lp/mm resolution across a 0.70-mm field of view in the SMC channel. The endoscope can perform high contrast crypt visualization, molecular imaging, and cross-sectional imaging of colon microstructure. © 2012 Society of Photo-Optical Instrumentation Engineers (SPIE). [DOI: 10.1117/1.JBO.17.8.086003]

Keywords: optical coherence tomography; surface magnifying chromoendoscopy; endoscope; catheter; gradient-index; gastrointestinal; colon; aberrant crypt foci.

Paper 12161P received Mar. 8, 2012; revised manuscript received Jul. 6, 2012; accepted for publication Jul. 12, 2012; published online Aug. 3, 2012.

1 Introduction

Colonoscopy is the most commonly used technique for early detection of colorectal cancer, which is the third most frequently diagnosed malignancy in the United States. In 2012, it is estimated that colorectal cancer will be responsible for 9% of newly diagnosed cancers as well as cancer related deaths in men and women. While the five-year survival rate is 90% when these cancers are detected at an early, localized stage, only 39% of patients are diagnosed early.¹ A need exists for rapid, nondestructive visualization of tissues *in vivo*, for clinical diagnostics as well as for scientific study in order to make significant advances in the basic science of chemoprevention and chemotherapy.

Optical coherence tomography (OCT) is a noninvasive interferometric imaging technique capable of imaging up to 2 mm deep in tissue. OCT creates cross-sectional images using near-infrared light back scattered from index of refraction mismatches.^{2,3} Recently, OCT has been used to image the human and mouse colon and rectum with micron-scale resolution.^{4,5} Various mouse models exist which are excellent platforms for studying colon carcinogenesis, preventatives and treatment methods.⁶

We have previously constructed dual modality endoscopes that provide OCT information about tissue boundaries, structure, and thickness, as well as laser-induced fluorescence (LIF) spectra information about the biochemical composition of the tissue. These endoscopes can provide a heightened sensitivity and specificity to tumor detection when compared to either modality alone.^{7,8} However, our current systems cannot reliably visualize the subtle alterations in mouse mucosal crypt structure

that signify the earliest stages of disease. Our OCT systems have sufficient resolution, but resolution is generally measured with a 100% contrast target. The innate contrast of the mouse colon is very low, which when combined with the very small crypt sizes, lead to challenges in colon visualization in this diminutive species. Exogenous contrast agents would mitigate this problem. We have utilized nanoshells as an OCT contrast agent in the mouse colon but they enhanced regions of tissue rather than crypt structure.⁹ Exogenous dyes could improve contrast, but our previous LIF systems have emphasized obtaining high resolution spectral rather than high resolution spatial information.

Surface-magnifying chromoendoscopy (SMC) has been developed to visualize the surface mucosal structure of the gastrointestinal (GI) tract, and has gained wide-ranging application for early detection of colorectal cancer and its precursors.^{10,11} Methylene blue (MB) is a dye clinically used to enhance contrast for SMC. MB can be visualized either by its significant absorption or fluorescence emission in the red to near-infrared wavelength range. With SMC, it is possible to discriminate normal colonic crypt structure from aberrant crypt foci (ACF). ACF are clinically interesting because the conventional paradigm is that they are the first event in colorectal carcinogenesis, although this paradigm has recently been debated.^{12,13} While studies to prove or disprove the role of ACF in humans are difficult, mouse models offer an opportunity to determine the causal relationship between ACF and colorectal neoplasia.

Combining SMC and OCT in one endoscopic system will allow the possibility for a large scale serial study to be done on the murine model, with SMC providing surface visualization of ACF and OCT allowing cross-sectional imaging for the

Address all correspondence to: Jennifer K. Barton, The University of Arizona, College of Optical Sciences, 1630 E. University Boulevard, Tucson, Arizona 85721. Tel: +520-621-4116; E-mail: barton@u.arizona.edu

detection of mucosal thickening and adenoma. We have designed a dual modality fluorescence-based SMC and OCT endoscope capable of resolving crypt structure in the mouse colon. In this paper, we describe our instrument for obtaining simultaneous fluorescence SMC and OCT data and present preliminary results obtained from methylene blue-stained mouse colon.

2 Materials and Methods

2.1 Proximal SMC-OCT System

A diagram of the SMC-OCT system is shown in Fig. 1. The optical paths of each modality are separated proximally, but combined distally in the sample arm. The fluorescence-based SMC proximal subsystem contains the excitation light source, optics for coupling this excitation light into the fiber bundle, filtering out the emission light, and imaging onto a charge coupled device (CCD) camera. Dichroic and emission filters are optimized to the emission peak of the methylene blue contrast agent and the use of a 638-nm laser diode source (Fiber-tec II, Blue Sky Research, Milpitas, CA).¹⁴ The laser source was coupled into the system via a single-mode fiber with a numerical aperture (NA) of 0.11. Light exiting this laser source fiber was collected with a 25-mm focal length lens, reflected off of a long-wave pass (LWP) filter centered at ~ 650 nm (HQ655LP, Chroma Technology Corp., Bellows Falls, VT), and focused at the entrance pupil of a 20 \times , 0.40 NA microscope objective (PLN 20X, Olympus America, Center Valley, PA). This arrangement allowed for Kohler illumination of a coherent imaging fiber bundle (IGN-08/30, Sumitomo Electric USA, Torrance, CA), which relayed light to the distal endoscopic optics (discussed below). Laser power on the sample was 8 mW. Emission light collected by the distal optics was relayed back to the proximal optics via the same fiber bundle. The proximal face of

the fiber was imaged onto the CCD camera (PIXIS 1024, Princeton Instruments, Trenton, NJ). The emission light transmits through the dichroic filter, and excitation light is further suppressed by a long pass emission filter (ZQ633RDC, Chroma Technology Corp., Bellows Falls, VT) placed directly in front of the CCD. SMC images were acquired with integration times between 15-100 ms, with a readout time of 250 ms.

2.1.1 Spectral domain OCT

The OCT subsystem has been previously described in detail.⁹ The source is a superluminescent diode (Broadlighter D-890, Superlum, Moscow) with a center wavelength of 890 nm and a full width half maximum (FWHM) bandwidth of 150 nm. The light is split using a 50:50 fiber beamsplitter in to a reference arm fiber and a sample arm fiber, which transmits light to the distal endoscope optics (discussed below) and illuminates the sample with 1.7 mW. The reference arm contains a 0.6 neutral optical density filter, a pair of SF2 right-angle prisms to compensate for dispersion in the sample arm optics, and a retro-reflecting mirror. Light returning from the sample and reference arms is recombined at the fiber-optic beam splitter. In the detector arm, light is dispersed in wavelength and focused onto a 2048-pixel CCD array using a custom-built spectrometer. OCT images are acquired at a rate of 4000 A-scans/s while the probe moves at a velocity of about 4.75 mm/s, corresponding to a spacing of 1.2 microns between samples.

2.2 Endoscope Design

2.2.1 Colon microscopy and fiber bundle

Fluorescence microscope images of the mouse colon crypt structure were obtained in order to determine the required resolution of the SMC subsystem. *Ex vivo* images of methylene

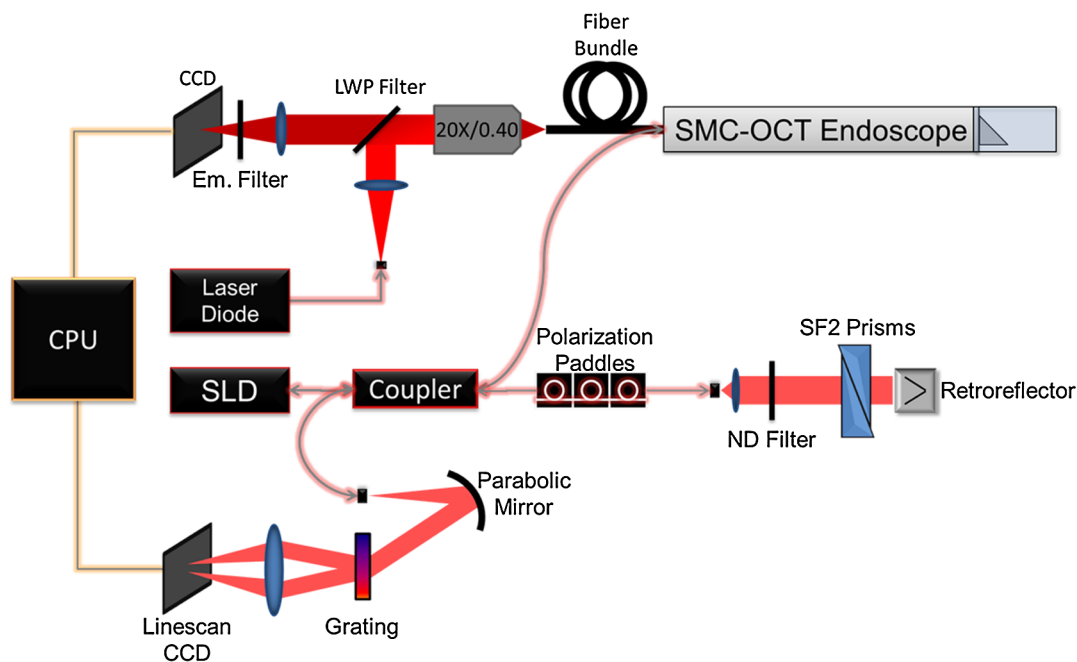


Fig. 1 Diagram of dual modality set up. Surface magnifying chromoendoscopy (SMC, 638-nm laser diode) and optical coherence tomography [OCT, 890-nm center wavelength superluminescent diode (SLD)] sources are fiber coupled into endoscope. A long-wave pass (LWP) filter is used to reflect excitation light and pass emission light in the SMC proximal setup, while neutral density (ND) filters attenuate OCT source power. Charge-coupled devices (CCD) are used to detect signal in each modality, and data is electronically transmitted to the central processing unit (CPU).

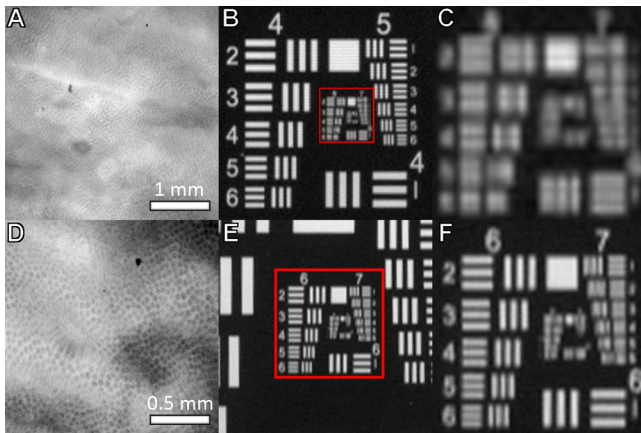


Fig. 2 Microscopic methylene blue stained *ex vivo* mouse colon and USAF bar target images viewed at 2 \times (a) and (b) and 4 \times (d) and (e). Mucosal crypt structure was resolved between the two sets of images, indicating a desired surface magnifying chromoendoscopy modality imaging resolution between 102–128 lp/mm. Parts (c) and (f) show enlarged views of boxed regions in parts (b) and (e), respectively.

blue-stained colon samples were compared against a US Air Force (USAF) bar target at varying microscope magnifications (Fig. 2); the crypt structure was easily visualized at a resolution of at least 65 lp/mm, and no further visualization enhancement was perceived after 145-lp/mm resolution.

Because the SMC subsystem utilizes a fiber bundle to transmit an image of the tissue to a CCD, both the proximal and distal optics must be carefully designed. The fiber bundle and distal optics assembly must be capable of sampling the tissue at a desired resolution, and the proximal optics and CCD must be capable of sampling the fiber bundle so that each core of the fiber bundle is imaged to at least 2 pixels in both the vertical and horizontal directions. For coherent fiber bundles, resolution of the system is limited by the core-to-core spacing of the individual fibers. For this application a 30,000-element, 0.72-mm clear aperture fiber bundle was selected with a core-to-core spacing of 4 μm (IGN-08/30, Sumitomo Electric USA, Torrance, CA), allowing for a bare-fiber bundle maximum imaging resolution of spatial frequencies based on twice this sampling rate: 8 μm or 125 lp/mm.¹⁵ Emission light was collimated by the proximal 20 \times objective and refocused on the detector by a simple 60-mm focal length achromatic doublet. This proximal setup imaged the fiber bundle to approximately 60% of the area of the 1 megapixel CCD. Thus each fiber was oversampled with approximately 3.25 pixels. Images taken of a USAF bar target placed at the distal end of the fiber bundle confirmed the ability of the bundle and proximal optics to resolve 125 lp/mm (Fig. 3).

2.2.2 SMC distal optics

Optical assemblies placed at the distal end of the fiber bundle can provide the magnification necessary to increase spatial resolution, at the expense of field of view. The inherent resolution of the fiber bundle was greater than the minimum necessary to visualize crypt structures, therefore the distal optics only needed to achieve a 1 \times magnification. Gradient-index (GRIN) lenses have been used in endoscopic imaging to robustly and simply focus light, but these systems are all forward-viewing.^{16–18} For the SMC subsystem, a side-viewing system was necessary for visualization of the mouse colon. A unique, side-viewing

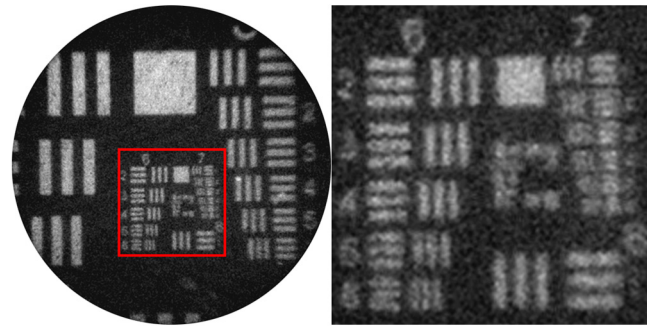


Fig. 3 Image taken of a USAF bar target, trans-illuminated with white light. Image confirms a fiber bundle resolution innately capable of resolving the first element in group 7 (128 lp/mm), an acceptable resolution to visualize the mucosal crypt structure of the mouse colon.

GRIN-based distal optics assembly was designed for this purpose.

The center wavelength-dependent index of refraction, gradient constant, and pitch or lens length of a GRIN lens affects its working distance, focal length, and NA. Manipulation of these GRIN assembly parameters enables customization for a variety of applications. In designing the SMC system, accommodations had to be made for the large numerical aperture, NA = 0.35, of the fiber bundle, and the design criterion of a 1:1 imaging system at a specific working distance. A GRIN lens diameter of 1.8 mm, compared to the 0.72-mm clear aperture of the fiber bundle, prevented vignetting of the excitation beam while allowing the full assembly to be placed inside a protective glass envelope with an inner diameter of 1.9 mm and outer diameter of 2.3 mm.

In order for the probe to be side-viewing, an additional element was needed to reflect light out of the circumference of the glass envelope. A simple aluminized right-angle prism made of BK7 was chosen with a leg dimension (1 mm) that allowed for the entire prism to be contained within the diameter of the cylindrical GRIN lens. The side-viewing working distance of the endoscope was then calculated to have a 1.58-mm air-equivalent optical path length (OPL), necessary to image the tissue through the right-angle prism, the air gap between the distal face of the prism and the glass envelope, and the 0.2-mm thick envelope wall.

GRIN lenses are capable of providing a specific front (distal) working distance with a fiber bundle placed at their proximal face by altering their pitch, but their distal-to-proximal magnification will be less than one. By introducing space between the fiber bundle and GRIN lens, a precise magnification can be achieved at a desired working distance. In practice, this was achieved by introducing a glass spacer. To achieve a 1 \times magnification at an OPL of 1.58 mm, a custom GRIN lens with a 1.8-mm diameter, based on the commercial GT-LFRL-180-025-50-CC lens (GRINTECH, Jena, Germany), was chosen with a center index of refraction at 670 nm, $n_0 = 1.629$, gradient constant, $g \sim 0.647$, and length, $l_{\text{GRIN}} = 5.41$ mm, along with a BK7 spacer of the same diameter that had a length, $l_s = 1.828$ mm.

To avoid possible total internal reflection (TIR) of light emitted from the tissue and collected by the prism, an aperture with a clear aperture, CA = 0.7 mm, and an outer diameter, $d = 1.8$ mm, was added to the distal optics assembly between the GRIN lens and the right-angle prism, effectively decreasing the size of the entrance pupil to the GRIN lens. An optical model

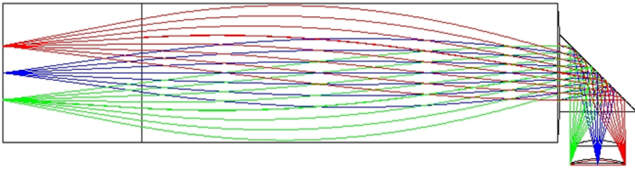


Fig. 4 Optical model of distal optics gradient-index (GRIN) lens-based assembly. System provides a magnification of 1 at a working distance of 1.58 mm, resulting in an imaging system that is theoretically capable of resolving 125 lp/mm across a 0.70-mm field of view.

of the SMC modality for the full distal assembly can be seen in Fig. 4.

2.2.3 OCT design

OCT light, which requires a focused NIR beam, also had to be relayed from the proximal optics to the tissue. In general, with OCT utilizing a longer wavelength of light and fibers with a smaller NA, the aforementioned GRIN assembly should provide for a deeper focal depth when compared to SMC light. To use the same distal optics for the two modalities, and with the fiber bundle occupying the inner diameter of the assembly, the effect of off-axis OCT fibers was modeled. Using 780-HP fiber (Nufern, East Granby, CT) with a cladding diameter of 125 μm to transmit the 890-nm center wavelength light, fiber placements were modeled around the outer circumference of the fiber bundle cladding at a radial position, $r = 462.5 \mu\text{m}$. It was observed that regardless of the fiber placement, all OCT light propagated through the system without vignetting, and was focused inside the tissue. A tradeoff between focal depth and resolution was observed as fibers were modeled from the 12 o'clock position

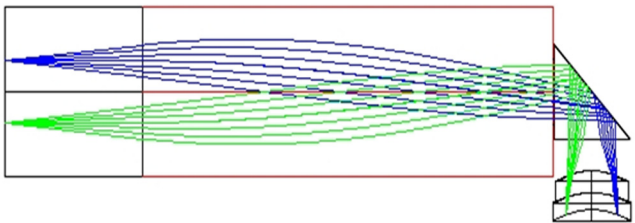


Fig. 5 Optical model of optical coherence tomography (OCT) light propagating through the distal assembly and being focused inside the tissue for fibers placed around the circumference of the fiber bundle cladding at the 1:30, 4:30, 7:30, and 10:30 positions. All four fiber placements have a similar focal depth and spot size.

to the 3 o'clock position and further down to the 6 o'clock position. When fibers were placed at the 12 and 6 o'clock positions, light focused 110 μm into the tissue with a diffraction-limited spot size of 3.9 μm . When the fibers were placed at 3 and 9 o'clock positions, OCT light focused 280 μm into the tissue with a spot size of 6.6 μm

As seen in Fig. 5, 1:30, 4:30, 7:30, and 10:30 fiber positions were settled upon, as they provided a focal depth of 190 μm , highly appropriate for the thin mouse colon, had a depth of focus of 70 μm , and still maintained a diffraction-limited, 3.9- μm OCT spot size. Once the light from these four fibers has propagated through the system, the spots are separated by 660 μm in the lateral direction, and 740 μm in the azimuthal direction. These positions were also chosen as to help with the mechanical construction of the endoscope, to be discussed subsequently.

2.3 Mechanical Design and Construction

Mechanical diagrams of the SMC-OCT endoscope can be seen in Fig. 6. Distal optics assemblies were first constructed, after which the problem of fastening the assembly to the fiber bundle and OCT fibers was managed. In order to secure the fibers to the proximal end of the spacer, a ferrule was fabricated with an outer diameter equal to that of the spacer and GRIN lens, and an open inner diameter, $d = 1.1 \text{ mm}$, which allowed sufficient space for two OCT fibers to flank the fiber bundle's diameter—using four OCT fibers total at 90-deg. increments around the circumference of the bundle—with 50- μm tolerance, enough for fibers to be precisely arranged in their respective positions before being cemented. For ease of construction, ferrules were also fabricated with a proximal lead-in. To assure proper spacing of the OCT fibers around the fiber bundle circumference, and centering of the fiber bundle assembly, 125- μm thick shims were placed in the ferrule in between the four OCT fibers.

Elements were secured together with a UV curing epoxy (OG603, Epoxy Technology, Billerica, MA) with an index of refraction ($n = 1.47$) that allowed for the minimization of back reflections. Proximal to the ferrule, fibers were protected with polyimide tubing with an inner diameter of 1.45 mm and a wall thickness of 57 μm (B0013H0X8E, SmallParts, Seattle). The full assembly was inserted into an outer assembly consisting of the glass envelope fixed to polyimide tubing with an inner diameter of 2.23 mm and a similar wall thickness (B0013HR0I4).

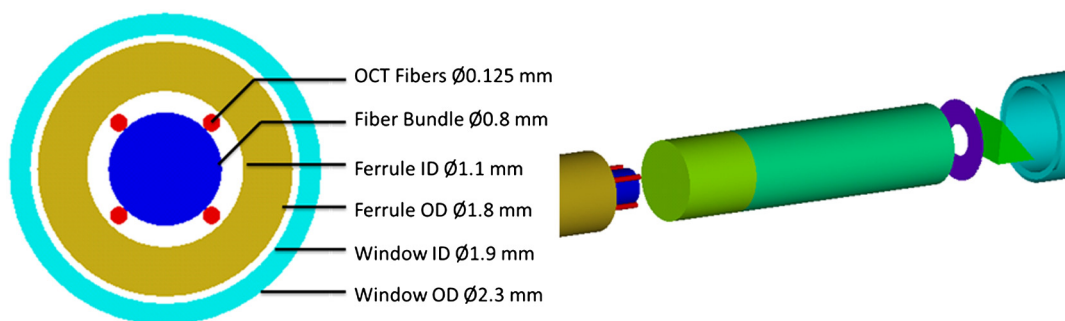


Fig. 6 Mechanical design of the surface magnifying chromoendoscopy-optical coherence tomography (SMC-OCT) endoscope. Four OCT fibers were placed symmetrically around the circumference of the fiber bundle, allowing for the centering of the fiber bundle in the ferrule, while also leading to a good focal depth and diffraction-limited spot size for OCT light in the tissue.

2.4 Animal Imaging

One C57BL/6 mouse was imaged to provide proof-of-concept of the operation of the combined OCT/SMC endoscopic imaging system. All studies were performed in accordance with a University of Arizona Institutional Animal Care and Use Committee approved protocol. Twenty-four hours prior to imaging, mice were fasted and given Pedialyte in place of water to clear the colon. Immediately prior to imaging, mice were anesthetized with a mixture of Ketamine (0.33 mg/ml, 100 mg/kg) and Xylazine (0.033 mg/ml, 10 mg/kg) administered by intraperitoneal (IP) injection. The colon was gently flushed with 3-9 mL of warm saline to clear excess mucous. Methylene blue (MB) solution (1%, 0.2 ml) was lavaged in the colon and allowed to incubate for 2 min, after which the colon was gently flushed again with warm saline. The SMC-OCT endoscope was coated with a thin layer of a biocompatible water-based lubricant and inserted approximately 32 mm inside the colon, and sequential SMC and OCT images obtained.

3 Results

3.1 Dual Modality Resolution

Once the system was constructed, SMC images were taken of a trans-illuminated USAF bar target to assess the image quality across the full field of view. The 6-5 and 7-1 elements were clearly resolved at four off-axis points in the image plane as well as the on-axis point, as seen below in Fig. 7, indicating

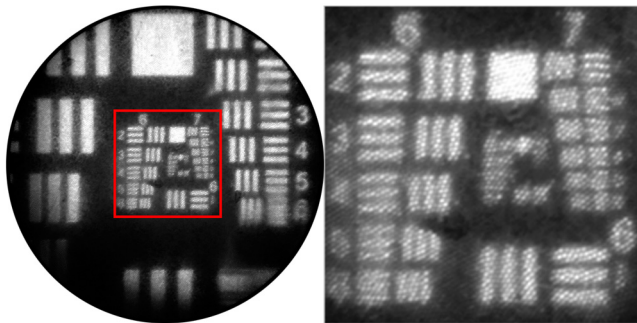


Fig. 7 USAF bar target trans-illuminated with white light and imaged by surface magnifying chromoendoscopy-optical coherence tomography (SMC-OCT) endoscope. 6-5 and 7-1 elements were clearly resolved at various points in the image plane, indicating a system resolution between 102-125 lp/mm.

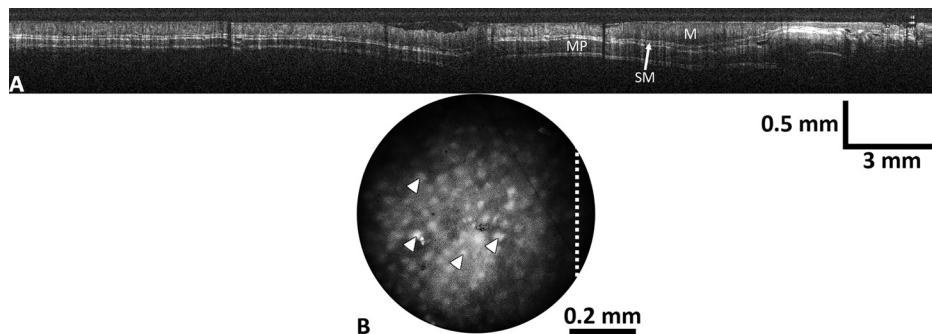


Fig. 8 Optical coherence tomography (OCT) image scanning the full 30 mm of the *in vivo* mouse colon (a), and surface magnifying chromoendoscopy (SMC) image taken at one location in the mouse colon (b). The layered structures of the colon, including mucosa (M), submucosa (SM), and muscularis propria (MP) are easily identified in the OCT image, while arrows in the SMC image point to individual colonic crypts, and the white dotted line corresponds to the scan line of the specific OCT image.

a SMC imaging resolution of 128 lp/mm, or 8- μ m Airy disk radius (see Appendix A).

For the OCT modality, an edge response method previously described in detail was used to calculate the experimental resolution of the constructed system.^{19,20} The FWHM lateral OCT resolution of the system was calculated to be approximately 4 μ m, which compares favorably with the theoretical value of 3.9 μ m.

3.2 Animal Imaging

Multiple images at 100-ms integration time were taken with the SMC modality, while the OCT channel scanned 30 mm of the colon at a rate of 4000 A-scans/s. Images for both modalities can be seen below in Fig. 8. Individual crypts are clearly resolved across the full field of view, as noted in the SMC image. In the second panel, a 20-mm long OCT image is presented, cropped from the original 30-mm long image, to highlight features of the *in vivo* mouse colon. The layered structures of the colon, including mucosa, submucosa, and muscularis propria, are easily identified. The line in Fig. 8(b) indicates the intersection of the orthogonal OCT image with the SMC image.

4 Discussion

A dual modality SMC-OCT endoscope was built capable of resolving the surface mucosal crypt structure as well as the morphological structure of the *in vivo* mouse colon. Meeting the simultaneous requirements of high resolution across a relatively large, curved, and precisely positioned SMC field of view, and high resolution for OCT imaging with an appropriate focal depth, was challenging and novel. To meet these specifications, precise control (and in some cases deliberate introduction) of chromatic aberration and astigmatism was achieved to create the required curved image field and OCT focal depth. Other nonstandard features include use of an annulus to reduce stray light, and unconventional use of off-axis OCT fibers to meet packaging constraints.

SMC images were taken as excitation light was relayed from an epi-fluorescence proximal setup into the endoscope via a 30,000-element, 0.72-mm clear aperture, 0.35-numerical aperture (NA) fiber bundle. Distal optics were designed to ensure a 1:1 imaging system at a specific side-viewing OPL of 1.58 mm. It is not uncommon for GRIN lens-based endoscopes to under achieve experimentally. One reason for this can be TIR of emitted light from the circumference of the GRIN

lens.²¹ For such a large NA fiber bundle it was decided that the GRIN assembly have a diameter larger than that of the clear aperture of the fiber bundle, as opposed to traditional microendoscopes that match the two diameters, in order to mitigate possible effects of total internal reflection (TIR) should excitation light interact with the circumference of the lens, as well as increase the excitation throughput of the system. Also, since fluorescence is isotropic, it was possible that emitted light could propagate back through the system at angles allowing for its TIR and subsequent collection at different individual fibers within the fiber bundle, increasing the background and hence decreasing the signal-to-background ratio necessary to achieve high resolutions. The annulus added to the system between the GRIN lens and right-angle prism sufficiently limits the aperture to prevent this effect.

Aberrations were induced in the system by the size, shape, and material of the various optical elements, and the gradient index of refraction of the GRIN lens. Unlike in typical OCT GRIN-based endoscopes, off-axis aberrations had to be considered in this design. As OCT light propagated from the fibers to the tissue, initial aberrations were induced at the spacer-GRIN lens junction in the form of spherical aberration. This spherical aberration was then compounded as OCT light continued to propagate off-axis through the GRIN media. However, the major source of OCT aberration in this system was at the prism-air interface. Light from each of the fibers exited the prism at an oblique tangential and sagittal angle, hence refracting into the air gap, inducing coma, astigmatism, and extra spherical aberration in the beam. Upon interacting with the cylindrical envelope—an effective negative lens in the azimuthal direction—coma, astigmatism, and spherical aberration were again induced only this time in the opposite direction from that before, and the overall beam quality was semi-corrected. To mitigate aberrations at the prism-air interface and yield a better-corrected system, various reflective elements were considered as alternatives to the rectangular prism, including miniature in-air mirrors and rod prisms with the same diameter as the GRIN assembly. Use of an in-air mirror offered little improvement, while the rod prism offered slightly increased performance. However, image quality was not increased to a sufficient degree to merit the fabrication of a custom piece.

OCT fiber placement was then derived as a result of the prism selection. While placement of the fibers at vertical positions (12:00 and 6:00) led to the best spot size and shallowest focal depth, horizontal fiber placements (3:00 and 9:00) led to above-diffraction-limited spot sizes with the deepest focal depth. This trade-off arose from the lack of system symmetry about the central optical axis. That is, while the system was axially symmetric during propagation through the spacer and GRIN lens, different optical path lengths through the prism, air gap, and cylindrical window let to an optical path difference between light from fibers placed at each of these directions, resulting in different focal depths and illumination numerical apertures. Interestingly, cancelling optical path length contributions from the tangential and sagittal directions led to light from each of the four fibers placed at the 1:30, 4:30, 7:30, and 10:30 positions having similar resulting beam characteristics. Resulting OCT light was focused 190 μm into the tissue with a diffraction-limited spot size and 70- μm depth of focus.

In the SMC channel, the same aberrations occurred. Whereas only one radial position had to be considered for the OCT fibers, the aberrations of the SMC subsystem had to be assessed across

the full field of view. Modeling the system with a flat exit window and flat object plane yielded a high level of field curvature and distortion induced primarily by the GRIN lens. Upon introduction of the cylindrical envelope and a cylindrical object plane, initial field curvature and distortion were overcorrected in the azimuthal direction but well-corrected in the longitudinal direction. Therefore, rather than the object plane being the ideal cylindrical surface, following the outer diameter of the glass envelope, the surface was nearly a cylinder, but with a smaller radius. By introducing slight of defocus—a lengthening of the spacer—a compromise image plane was induced, which decreased the average image blur and assured that image quality (lp/mm resolution) was degraded no more than 20% from the optimum and no lower than initial imaging specifications.

Preliminary images were taken of the methylene blue-stained *in vivo* mouse colon with both modalities. The OCT and SMC channels of the endoscope are inherently coregistered, with approximately orthogonal imaging planes. The exact position of the intersection of these planes depends upon which OCT channel was selected. Due to the rapidity of OCT imaging compared to SMC imaging, the OCT and SMC data are obtained sequentially, with OCT acquired during longitudinal movement into the colon and SMC acquired during the pullback, then the endoscope optics are rotated to the next angular imaging location. During future time-serial mouse imaging studies, multiple SMC images will be merged to produce a complete surface map of the distal mouse colon. This surface map will compliment multiple cross-sectional OCT images obtained at various angles that sample the subsurface structure of the colon. Experimentally, this endoscopic system will allow for the observation of the prevalence of ACF within the mouse colon, and the monitoring of the onset of colorectal neoplasia in their early stages, enabling the current colon carcinogenesis paradigm to be tested.

Appendix: Resolution Conversion

A modulation transfer function contrast value of 9%, close to that which is seen in the 6-6 and 7-1 groups of the imaged USAF bar target in Fig. 7, is implied at the Rayleigh diffraction limit. Under this criterion, two features are resolved when the central maximum of one's Airy disk is located at the first zero of the other's. Feature separation is equal to that of one Airy disk radius. That is to say that if we are resolving 125 lp/mm with 9% contrast, the following conversion can be used:

$$125 \text{ line pairs/mm} = 0.125 \text{ line pairs}/\mu\text{m}$$

$$1/(0.125 \text{ line pairs}/\mu\text{m}) = 8 \mu\text{m/line pair}$$

$$8 \mu\text{m/line pair} = 8\text{-}\mu\text{m Airy disk radius}$$

$$= 8\text{-}\mu\text{m Rayleigh criterion resolution.}$$

Acknowledgments

This research was supported in part by National Institutes of Health (NIH) Grant No. R01 CA109835.

References

1. American Cancer Society, Cancer Facts & Figures 2012, <http://www.cancer.org/acs/groups/content/@epidemiologysurveillance/documents/document/acspc-031941.pdf>, American Cancer Society, Atlanta, GA (1 March 2012).

2. B. E. Bouma and G. J. Yearney, Eds., *Handbook of Optical Coherence Tomography*, Marcel Dekker, New York (2002).
3. D. Huang et al., "Optical coherence tomography," *Science* **254**(5035), 1178–1181 (1991).
4. D. C. Adler et al., "Three-dimensional endomicroscopy of the human colon using optical coherence tomography," *Opt. Express* **17**(2), 784–796 (2009).
5. L. P. Hariri et al., "Ex vivo optical coherence tomography and laser-induced fluorescence spectroscopy imaging of murine gastrointestinal tract," *Comp. Med.* **57**, 175–185 (2007).
6. E. W. Germer, N. A. Ignatenko, and D. G. Besselsen, "Preclinical models for chemoprevention of colon cancer," *Recent Res. Cancer* **163**, 264–266 (2003).
7. L. P. Hariri et al., "Serial endoscopy in azoxymethane treated mice using ultra-high resolution optical coherence tomography," *Cancer Biol. Ther.* **6**, 1752–1762 (2007).
8. J. K. Barton, A. R. Tumlinson, and U. Utzinger, "Combined endoscopic optical coherence tomography and laser induced fluorescence," in *Optical Coherence Tomography: Technology and Applications*, Eds., W. Drexler and J. Fujimoto, Springer, New York, NY (2008).
9. A. M. Winkler et al., "Quantitative tool for rapid disease mapping using optical coherence tomography images of azoxymethane-treated mouse colon," *J. Biomed Opt.* **15**, 041512 (2010).
10. K. Ohnita et al., "Magnifying chromoendoscopic findings of early gastric cancer and gastric adenoma," *Digest. Dis. Sci.* **56**(9), 2715–2722 (2011).
11. H. Chicho-Lach and K. Celinski, "Modern methods of endoscopic diagnosis of gastrointestinal tract," *J. Physiol. Pharmacol.* **58**, 21–31 (2007).
12. J. C. Anderson et al., "Aberrant crypt foci as predictors of colorectal neoplasia on repeat colonoscopy," *Cancer Cause. Control* **23**(2), 355–361 (2012).
13. N. L. Cho et al., "Aberrant crypt foci in the adenoma prevention with celecoxib trial," *Cancer Prev. Res.* **1**, 21–31 (2008).
14. T. J. Muldoon et al., "Subcellular-resolution molecular imaging within living tissue by fiber microendoscopy," *Opt. Express* **15**(25), 16413–16423 (2007).
15. J. B. Pawley, "Points pixels and gray levels: digitizing image data," in *The Handbook of Biological Confocal Microscopy*, 3rd ed., Springer Science+Business Media, New York (2006).
16. M. Pierce, D. Yu, and R. Richards-Kortum, "High-resolution fiber-optic microendoscopy for in situ cellular imaging," *J. Vis. Express* **47**, 3–6 (2011).
17. A. Latrive and A. C. Boccara, "In vivo and in situ cellular imaging full-field optical coherence tomography with a rigid endoscopic probe," *Opt. Express* **2**(10), 2897–2904 (2011).
18. S. Schenkl et al., "Rigid and high NA multiphoton fluorescence GRIN-endoscopes," *Proc. ECBO* **6631**, 1–7 (2007).
19. R. A. Wall, G. T. Bonnema, and J. K. Barton, "Focused OCT and LIF endoscope," *Proc. SPIE* **7558**, 75580Q (2010).
20. S. W. Smith, "Special imaging techniques," in *The Scientist and Engineer's Guide to Digital Signal Processing*, California Technical Publishing, San Diego (1997).
21. A. L. Kano, "Ultrathin single and multi-channel fiberscopes for biomedical imaging," PhD dissertation, (The University of Arizona 2009).